Pediatr Radiol (2017) 47:1031–1045
DOI 10.1007/s00247-017-3884-z

PEDIATRIC ULTRASOUND

Neurosonography: Assessing the Premature Infant

Vijetha V. Maller[1,2] · **Harris L. Cohen**[1,2]

Received: 5 January 2017 / Revised: 5 March 2017 / Accepted: 28 April 2017 / Published online: 2 August 2017

Abstract Neurosonography has proven to be helpful in neonatal brain diagnosis. Premature infants are at great risk for intraventricular hemorrhage and periventricular leukomalacia, key abnormalities affecting developmental outcome. Here we discuss technique, anatomy, variants and key points for diagnosis.

Keywords Brain · Germinal matrix · Hemorrhage · Hydrocephalus · Leukomalacia · Neonate · Preterm infant · Ultrasound

Introduction

A preterm infant is defined as a neonate born alive before the completion of 37 weeks of gestation. Extremely preterm (<28 weeks of gestation) and very preterm (28–32 weeks of gestation) infants have a higher mortality and morbidity because of their greater risk for intraventricular hemorrhage (IVH) and periventricular leukomalacia (PVL), which can lead to poor neurodevelopmental outcomes. Premature neonates have impaired cerebrovascular autoregulation, including pressure-passive cerebral circulation. Elevations in arterial or venous pressure lead to increases in cerebral blood flow and potential hemorrhage in the germinal matrix region, where there are fragile single-celled vessels as well as neuroblasts that normally migrate and develop as neurons in the peripheral gray matter. Episodes of hypotension result in reduced cerebral flow, hypoxia and reperfusion injury that can also result in germinal matrix hemorrhage [1]. Early diagnosis of hemorrhage allows for clinical neonatology efforts to minimize subsequent sequelae. Findings on follow-up ultrasound (US) can serve as a prognostic indicator for long-term neurodevelopmental outcome. The neurological manifestations of injury to the premature brain can range from cognitive defects to the major motor defects of cerebral palsy [2, 3].

History

In 1977 Burstein et al. [4], using CT, demonstrated a high percentage of intracranial hemorrhage in premature infants. Transport and the timing of CT imaging based on the clinical status of the neonate was an issue. In 1979–1980 the first descriptions of head US using the anterior fontanelle as a window led to practical real-time evaluation of the premature infant, at the bedside and within the isolette [5, 6]. In 1980 the first reports came of US detecting subependymal and intraventricular hemorrhage in premature infants [7]. Significant technical improvements in US and Doppler software and hardware have since allowed increased resolution and improved image quality as well as more sensitive vascular flow analysis, increasing our ability to diagnose abnormalities in the brain and surrounding structures of newborns and young infants.

✉ Vijetha V. Maller
vijethamaller@gmail.com

[1] Department of Radiology,
Le Bonheur Children's Hospital,
848 Adams Ave, Radiology G216, Memphis, TN 38103, USA

[2] Department of Radiology,
University of Tennessee Health Science Center,
865 Jefferson Ave, Suite F-150, Memphis, TN 38163, USA

Technique of head ultrasonography

A standard neonatal head US examination includes coronal and sagittal (midline and parasagittal) imaging using a transducer (usually a sector, vector or curved linear array) that fits the anterior fontanelle. The transducer choice is based on the trade-off between the excellent near-field resolution of a high-frequency transducer and the better penetration of a lower-frequency transducer. Images are best obtained with frequencies of 7.5 MHz or higher. Additional imaging might be performed through the posterior or mastoid fontanelle, and less often through any other open suture, craniotomy defect or the foramen magnum. Lower-frequency transducers can be used to take advantage of thinner areas of the temporal and parietal bones to obtain transcranial images of the brain. Posterior fontanelle views, when obtained via sagittal and coronal planes, have been noted to pick up a greater number of cases of neonatal hemorrhage by allowing improved evaluation of the contents of the atria and the occipital horns of the lateral ventricles [8, 9]. The mastoid fontanelle, located at the junction of the squamous, lambdoid and occipital sutures, behind the ear, does not fuse until 2 years of age. Imaging through it allows excellent visualization of the subtentorial intracranial structures (Fig. 1) including the cisterna magna, 4th ventricle, cerebellar hemispheres and cerebellar vermis, as well as the atrial and occipital portions of the lateral ventricles.

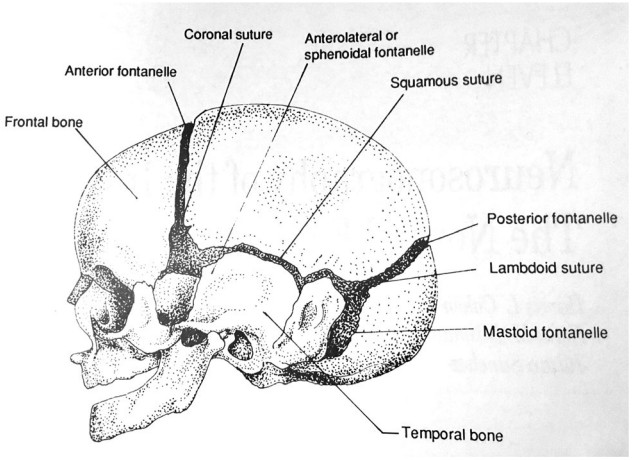

Fig. 1 Infant skull with normal open sutures. Diagram shows sutures that can serve as sonographic windows to the brain. The anterior fontanelle is used routinely. We also routinely use the mastoid fontanelle and occasionally the posterior fontanelle. Reprinted with permission from reference [10], p. 404

Anterior fontanelle views

Evaluating the brain in coronal plane

The transducer is angled from front to back, imaging the brain parenchyma from the orbit to subtentorium, with concentration on the ventricular system from its frontal horns through its body (Fig. 2). Frontal, temporoparietal and occipital portions of the supratentorial brain are assessed and, to a lesser extent, so are the subtentorial structures. Ventricular size can be evaluated at the level of the frontal horns and the body of the lateral ventricles. Homogeneously echogenic choroid, the major site of cerebrospinal fluid (CSF) production, is seen within the lateral ventricles. The corpus callosum is seen on coronal views as anterosuperior to the frontal horns. Its posterior portion is seen posterior to the bodies of the lateral ventricles. Inferior to the corpus callosum, the medial walls of the frontal horns contain a potential space between the septi pellucidi that is known as the cavum septum pellucidum. A cavum septum pellucidum is seen in at least 90% of all preterm neonates and 60% of full-term infants, usually closing at 2–6 months after birth [11]. At times during the exam in the coronal plane, particularly if there is poor seating of the transducer in the fontanelle from, for example, prominent hair, it might be difficult to see the periphery of the frontal brain well. In such cases, moving the transducer to the extreme right or left of the anterior fontanelle and angling it toward the contralateral side might help to assess the gray and white matter and also the extra-axial spaces of the peripheral brain on that side. At the brain peripheries are the Sylvian fissures, which might have a somewhat wider rectangular shape in very premature babies

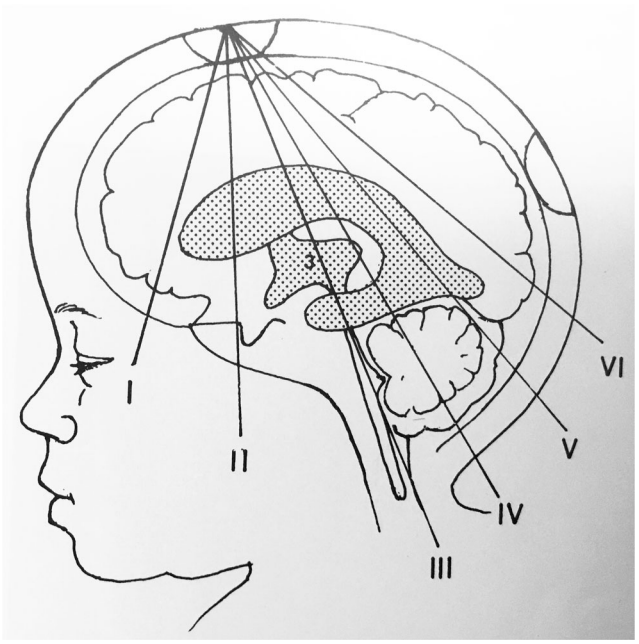

Fig. 2 Normal coronal planes of head ultrasound. Diagram depicts how the transducer, placed at the anterior fontanelle, is angled from front to back, imaging the brain parenchyma from the orbit to subtentorium with concentration on the ventricular system from its frontal portion through its body. Reprinted with permission from reference [10], p. 413

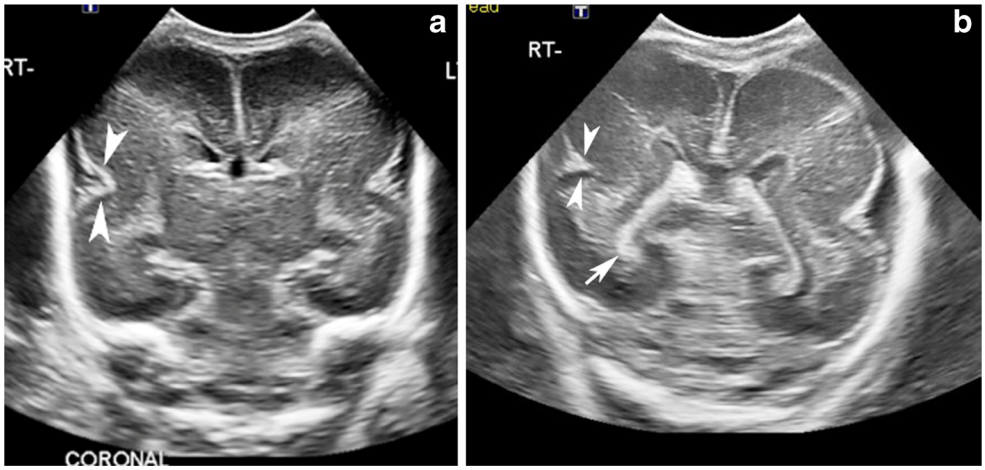

Fig. 3 Normal Sylvian fissure in a premature neonate. Head US imaging in coronal plane in a 5-day-old premature girl who was born at 24 weeks of gestation. **a** Level through frontal horns shows the right Sylvian fissure (*arrowheads*), which appears triangular with echoless cerebrospinal fluid (CSF) lateral to it. The Sylvian fissure appears more prominent than what would be seen in an older neonate, where it appears as a linear echogenic Y-shape. This is a result of lesser amounts of brain at this age. Note the lack of prominent gyri or sulci, consistent with what is expected for this premature neonate. **b** Level through body of lateral ventricles. This image was obtained through a greater degree of posterior angulation than (**a**). Only a few gyri and sulci are seen, consistent with the neonate's early 24-week gestational age. We have called this the "toast" sign. Agyria cannot be diagnosed at this age. Note the Sylvian fissure (*arrowheads*) of this very premature brain, which is almost a V-shape, with prominent extra-axial fluid indicating lesser brain development at this time. The homogeneously echogenic choroid plexus (*arrow*) lies within the right lateral ventricle. No prominent intraventricular CSF is seen lateral to it to suggest ventricular enlargement

because lesser brain parenchyma is often present (Fig. 3) as compared to the classic echogenic Y shape seen in the brain of a term infant [12] (Fig. 4).

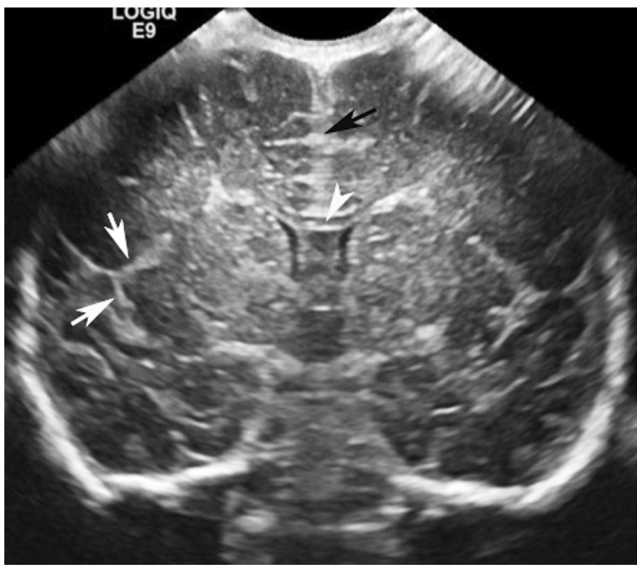

Fig. 4 Normal head US imaging in a 4-week-old boy born at 35 weeks of gestation. Coronal plane through the level of frontal horns shows the Y-shape Sylvian fissure (*white arrows*) on the right. At this gestational age there are greater amounts of brain on either side of the fissure compared to the neonate in Fig. 3. The frontal horns are normal in size. Note the anterior corpus callosum (*arrowhead*), which is hypoechoic compared to the interhemispheric fissure. The interhemispheric fissure is seen superiorly as an echogenic linear structure (*black arrow*). This, along with the linings of the medial brain, is often called the anchor sign. In cases of volume loss or extra-axial fluid at this site, the area appears echoless centrally

Evaluating the brain in sagittal and parasagittal planes

The midline sagittal plane allows the complete visualization of the corpus callosum (Fig. 5). It is seen superior to the cavum septum pellucidum, which might extend posteriorly as the cavum vergae. In some cases, this CSF-filled area extends even more posteriorly, beyond the bodies of the lateral ventricles and projecting beyond the quadrigeminal cistern as the cavum velum interpositum [13]. The echogenic pericallosal sulcus, which contains the pericallosal arteries, surrounds the corpus callosum superiorly. The pericallosal sulcus is surrounded

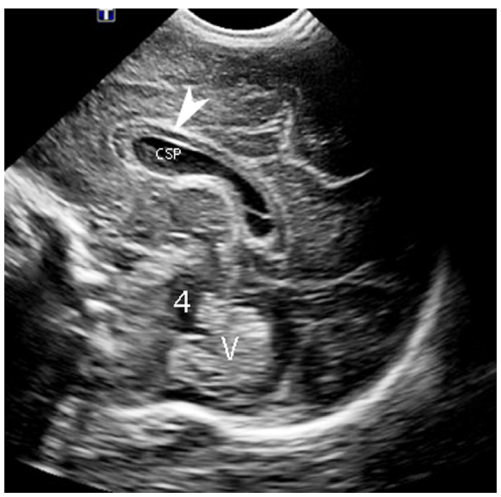

Fig. 5 Normal head US examination in the sagittal plane through the midline in a 4-week-old boy born at 35 weeks of gestation. The echoless cavum septum pellucidum (*CSP*) extends posteriorly as the cavum vergae and cavum velum interpositum. It sits below the corpus callosum (*arrowhead*). *4* 4th ventricle, *V* cerebellar vermis

superiorly by the cingulate gyrus. The number of gyri and sulci seen as echogenic lines in the brain increases with gestational age [14]. Very few gyri and sulci are normally seen earlier, i.e. at 24–28 weeks, limiting the ability to diagnose lissencephaly. In the midline the 3rd ventricle is seen well only if exactly midline or if it is enlarged. The 3rd ventricle is seen inferior to the corpus callosum and cavum septum pellucidum. Choroid plexus can be seen normally in the roof of the 3rd ventricle [10]. Color Doppler performed in midline sagittal view shows the anterior cerebral artery crossing over and paralleling the corpus callosum. If no corpus callosum is present, the artery's course would be superior, at a position anterior to the expected position of the anterior corpus callosum.

Parasagittal views of each side of the brain are obtained by angling the transducer laterally from the midline (Fig. 6). Occasionally it is helpful to move the transducer peripherally to the left of the anterior fontanelle and angle to the right to see the right lateral ventricle better and vice versa. Each lateral ventricle should be evaluated for its frontal horn, body, atrium (the first area to dilate in hydrocephalus) and occipital horn. The choroid plexus is well seen on parasagittal views within the lateral ventricles. It can at times have a lobular or bulbous appearance. Its homogeneously bright echogenicity can be confused with IVH. However, three points can help differentiate choroid plexus from IVH. The normal choroid plexus does not extend into the occipital horns or anterior to the foramina of Monro. The choroid plexus remains echogenic, while hemorrhage becomes less echogenic over time, as the clot lyses. Color Doppler shows the choroid plexus to have contained vascular flow by color Doppler, whereas clot has no vascular flow. Peritrigonal echogenicity, also known as the peritrigonal halo or blush, can be seen in the parenchyma in the peri-atrial area. It suggests white matter abnormality. However, the prominent echogenicity is caused by anisotropic effect from the US beam striking exactly perpendicular to the white matter tracts when insonated via an anterior fontanelle approach [15] (Fig. 7). The key parasagittal image searched for on each side of the head is the germinal matrix region where the head of the caudate nucleus and the thalamus meet, the caudothalamic groove (Fig. 8). By the time a neonate is viable, its germinal matrix is usually contained in this area. The germinal matrix region is larger far earlier in fetal life. It is in this area that neuroblasts and single-cell vessels sit and subependymal hemorrhage can develop. Routine parasagittal imaging continues with angulation to the brain periphery and the Sylvian fissure, where Doppler can show its contained middle cerebral artery tributaries (Fig. 9).

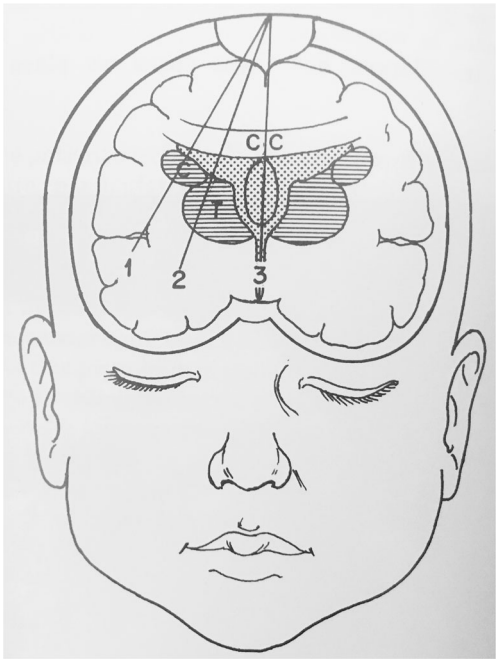

Fig. 6 Median and paramedian planes. Diagram shows plane 1 extending through the Sylvian fissure at the brain periphery. Plane 2 runs through the head of caudate (*c*) and thalamus (*T*). Plane 3 extends through the midline. *CC* corpus callosum. Reprinted with permission from reference [10], p. 406

Mastoid view

The posterior fossa structures are best visualized on transmastoid views. The midbrain with its contained aqueduct of Sylvius is seen as a hypoechoic structure caudal to the thalamus. If enlarged, the aqueduct, like all CSF-containing structures, appears echoless. Key information obtained on these views is the anatomy of the

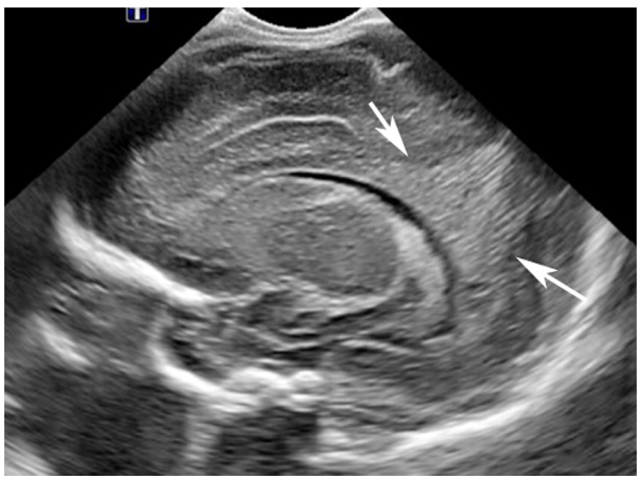

Fig. 7 Peritrigonal echogenicity caused by anisotropy. Head US examination in the parasagittal plane in a 3-day-old girl born at 26 weeks of gestation. There is an echogenic area in the peritrigonal region (*arrows*) that could simulate echogenic periventricular leukomalacia but is caused by normal white matter fibers lying at a 90° angle to the sound sent from the transducer placed in the anterior fontanelle. This creates an anisotropic effect responsible for the apparent greater echogenicity of these normal structures

Fig. 8 Normal head US examination in the parasagittal plane through the right germinal matrix region in a 4-day-old boy born at 32 weeks of gestation. US shows echoless cerebrospinal fluid in the body of the right lateral ventricle (*arrowheads*). Note the homogeneously echogenic choroid (*arrow*) in the atrium of the lateral ventricle. The caudate head (*C*) and the thalamus (*T*) meet at the caudothalamic groove. This area must be reviewed for any evidence of bright (when acute) germinal matrix hemorrhage

cerebellar hemispheres, seen as ovoid hypoechoic structures caudal to the echogenic tentorium (Fig. 10). They are symmetrical, with each containing bright areas of echogenicity consistent with the folia of the hemispheres. In many cases, it is only the hemisphere closest to the transducer that is technically best seen and its folia most apparent. The cerebellar vermis appears as an echogenic midline structure between the hemispheres. The anechoic cisterna magna is seen posterior to the vermis and cerebellar hemispheres, while the 4th ventricle is anterior to the vermis [16]. The foramen of Magendie can sometimes be seen in a normal brain at the inferior portion of the cerebellum, as an echoless area extending between the 4th ventricle and the cisterna magna (Fig. 10). Classic Dandy–Walker malformation shows communication between the cisterna magna and the 4th ventricle because of the association with vermian dysgenesis. Further discussion of Dandy–Walker malformation is beyond the scope of this review.

Germinal matrix hemorrhage

Germinal matrix hemorrhage is the most commonly diagnosed abnormality in the premature brain. The germinal matrix, as already stated, is an area of neuronal and glial cell proliferation with a rich single-celled vascularity. Early in gestation it lines the entire ventricular system. Neuroblasts from this area migrate toward the periphery of the brain during its development [4, 17]. The germinal matrix begins to involute by the end of second trimester, and by 28–32 weeks only a small amount of germinal matrix remains, essentially at the caudothalamic groove [2]. By 35–36 weeks, the germinal matrix involutes completely, which makes the risk of germinal matrix hemorrhage in near-term infants essentially very low. Systemic hemodynamic instability and immature cerebral blood pressure autoregulation are key factors in the development of hemorrhage at the germinal matrix area. This hemorrhage can extend into the ventricular system and when large can be associated with white matter infarction [1].

Papile and colleagues [18] classified the germinal matrix hemorrhage and IVH they saw on CT in 1978. In their classification, grade 1 hemorrhage is limited to the subependymal region, i.e. a subependymal hemorrhage; grade 2 hemorrhages include those with an intraventricular extension of the hemorrhage; grade 3 hemorrhages extend

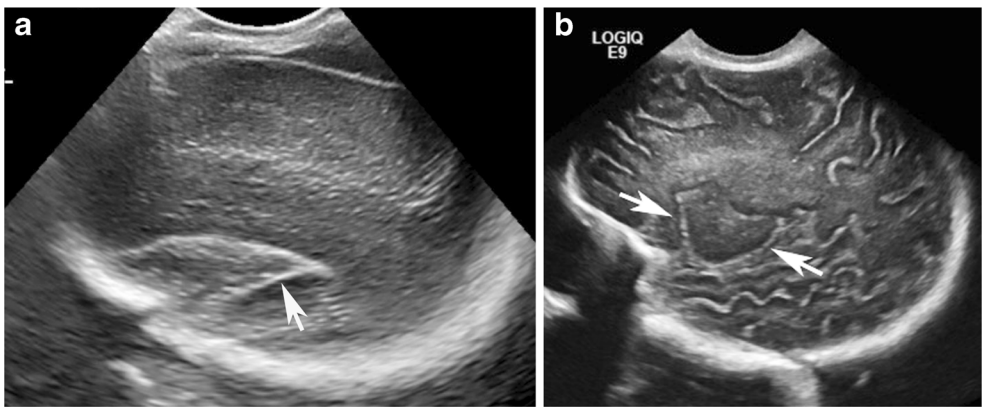

Fig. 9 Normal appearance of Sylvian fissure at different neonatal ages. Head US examination in the parasagittal planes at the brain periphery. **a** Younger premature. US shows the posterior aspect of a triangular- to quadrilateral-shape Sylvian fissure (*arrow*) in a girl born at 26 weeks of gestation. Lesser brain at the Sylvian fissure allows the fissure's cerebrospinal fluid to appear more prominent and maintain this shape. Lack of peripheral gyri underlines the neonate's early gestational age. **b** Older premature. US shows the Sylvian fissure (*arrows*) in a male neonate born at 36 weeks of gestation. Multiple gyri are seen. If Color Doppler were used, middle cerebral artery tributaries would be seen running in the vertically echogenic lines in the brain parenchyma at the Sylvian fissure

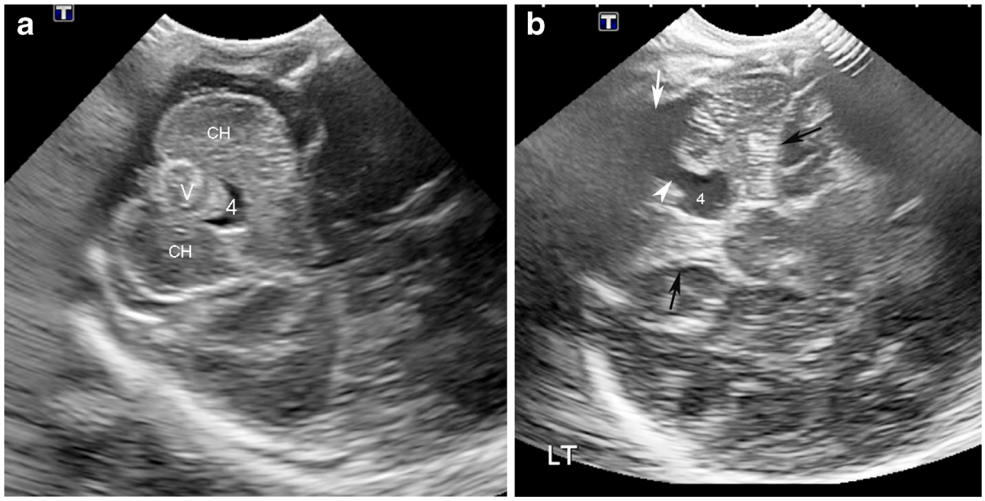

Fig. 10 Normal subtentorial contents. Head US examination, mastoid fontanelle views, in a 7-day-old girl born at 33 weeks of gestation. **a** Axial plane through the bodies of cerebellar hemispheres. Note the echogenic midline vermis (*V*), which sits just posterior to the normal 4th ventricle (*4*). Both right and left cerebellar hemispheres (*CH*) are well seen. **b** Plane through the inferior aspect of the cerebellar hemispheres. US shows an echoless structure, the foramen of Magendie (*arrowhead*), often seen at this site, particularly in the younger neonate; it extends to the 4th ventricle (*4*) from the cisterna magna (*white arrow*). This communication at the inferior aspect of the 4th ventricle is not indicative of inferior vermian hypoplasia. Note the tentorium (*black arrows*)

into the ventricles and cause prominent ventricular dilation. Grade 4 hemorrhages were at one time described as intraventricular hemorrhage extending directly into the brain parenchyma and resulting in associated intraparenchymal hemorrhage [17, 18]. However, Volpe [17] noted that the intraparenchymal component of the grade 4 IVH is not a result of direct extension of the bleeding but rather venous infarction that develops within 1–2 days of the prominent IVH. This infarction could develop because of the clot's mass effect and compression on the draining terminal veins as they pass near the germinal matrix [19, 20]. While the grading system has its limitations and its detractors, it is still used. A lower-grade hemorrhage in a child who later develops post-hemorrhagic hydrocephalus should not be subsequently given a higher grade. The short-term mortality rates for grades 1, 2, 3 and 4 hemorrhages are approximately 0–12%, 2–24%, 8–32% and 22–45%, respectively, and their long-term morbidity rates are 15%, 25%, 50% and 75%, respectively [2]. Early onset IVH, in the first 6 h after birth, has been associated with a higher risk for both cognitive and motor impairment than hemorrhages that occur later [21]. Obstetrical US and MR have shown that IVH can occur in fetal life as well [22, 23].

Intraventricular hemorrhage

Grade 1 hemorrhages are visualized in the germinal matrix region. This can be seen as an area of increased echogenicity inferolateral to the floor of the frontal horns and medial to the head of the caudate nucleus on coronal images, or between the head of the caudate and thalamus, or somewhat anterior to it on parasagittal imaging (Fig. 11). Large germinal matrix hemorrhages can elevate the floor of the lateral ventricles, resulting in the effacement of the frontal horn or body. The germinal matrix hemorrhage regresses in size over a period of time, as the clot lyses, and sometimes completely resolves. Often the subacute or older subependymal hemorrhage can be seen as a clot with cysts or cysts alone (Fig. 12). *Grade 2 hemorrhages* fill part or all of the ventricular system secondary to rupture of the germinal matrix hemorrhage through the lateral ependymal wall (Fig. 13). By definition the ventricle is not dilated to greater than 50% capacity. *Grade 3 hemorrhages* show intraventricular hemorrhage and prominent ventriculomegaly (Fig. 14). With any IVH, blood can fill and expand the 3rd and the 4th ventricles, and this typically appears homogeneously echogenic from when clot forms. As the hemorrhage evolves, the clot retracts and undergoes lysis, becoming heterogeneous in echogenicity and smaller in size. This can result early in the course of clot lysis, in a more echopenic (less echogenic) clot, often with some bright peripheral echogenicity (Fig. 15). IVH can usually result in ependymal lining echogenicity from what some have noted as a chemical ventriculitis, because of the irritant blood products, which gradually disappears in 6–8 weeks [24]. Increased echogenicity to the ependymal lining

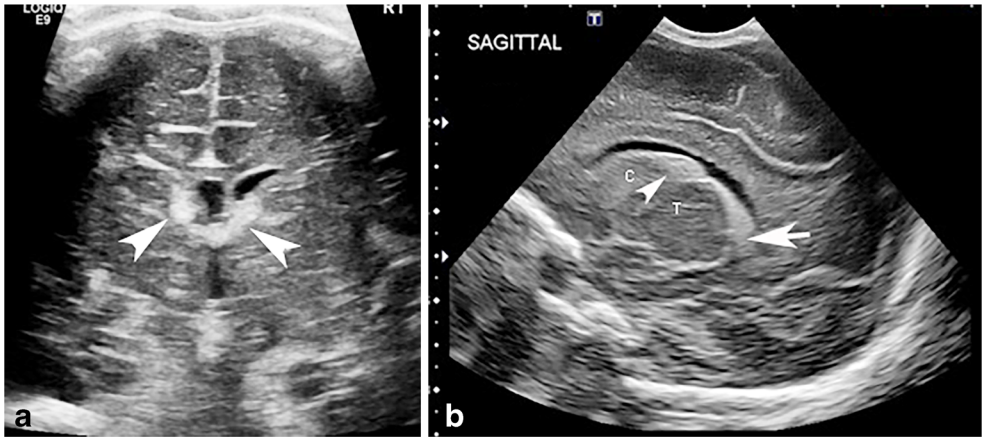

Fig. 11 Subependymal echogenicity of grade 1 hemorrhage. Head US examination in a 4-day-old boy born at 32 weeks of gestation. **a** In the coronal plane, US shows focal echogenicity (*arrowheads*) posterior and medial to the frontal horns. It is more clearly seen near the frontal horn on the left. The homogeneously bright echogenicity is consistent with early hemorrhage in the subependymal area between the caudate head and thalamus. Unlike grade 2 or higher hemorrhage, grade 1 hemorrhage is not seen within the ventricle. **b** US in the parasagittal plane shows bright echogenicity (*arrowhead*) in the orthogonal plane between the head of caudate (*C*) and thalamus (*T*). Note the normal choroid (*arrow*) in the lateral ventricle

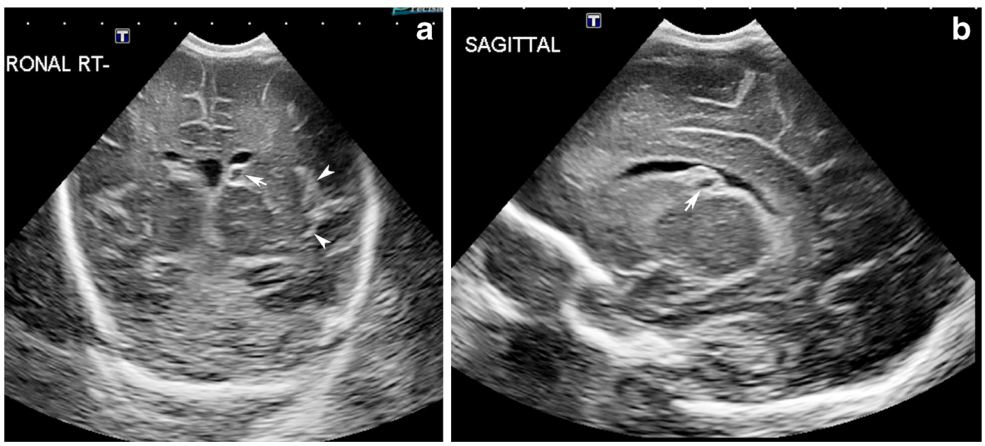

Fig. 12 Aging subependymal hemorrhage. Head US examination in a 14-day-old boy born at 31 weeks of gestation. **a** US in the coronal plane shows a focal, somewhat thick-walled cystic area (*arrow*) in the left subependymal area. It is echoless centrally and echogenic peripherally, consistent with an evolving subacute or older subependymal hemorrhage. Incidentally, note the Y-shape Sylvian fissure (*arrowheads*). A right-side subependymal hemorrhage is seen less well on this image. **b** US in the parasagittal plane shows echogenic mass with contained cyst (*arrow*), evidence of subacute or older subependymal cyst

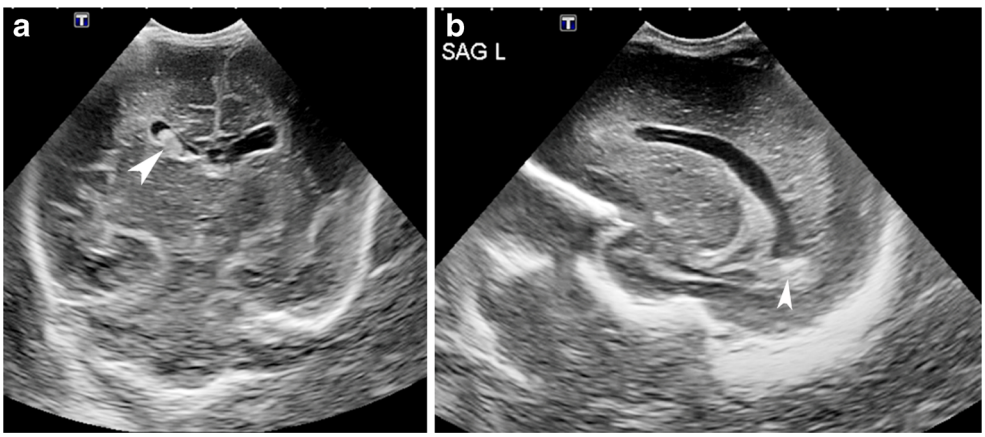

Fig. 13 Grade 2 intraventricular hemorrhage (IVH). Head US examination in a 7-day-old boy born at 28 weeks of gestation. **a** US in the coronal plane shows echogenic clot within the right frontal horn (*arrowhead*). There is no prominent dilation of the ventricle. **b** US in the left parasagittal plane shows clot (*arrowhead*) in the dependent portion of the atrium of a not prominently dilated lateral ventricle

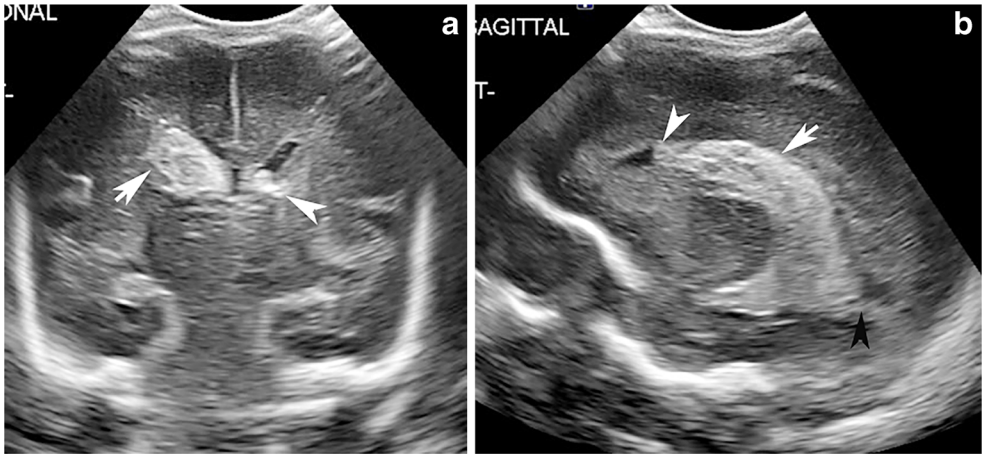

Fig. 14 Grade 3 intraventricular hemorrhage (IVH). Head US examination, coronal plane, in a 5-day-old girl born at 24 weeks of gestation. **a** US imaging shows a slightly heterogeneous large clot (*arrow*) in the right frontal horn. The prominent ventricular dilation suggests a grade 3 right IVH. Note the smaller clot (*arrowhead*), probably within a non-dilated left frontal horn, and the germinal matrix area equivalent to grade 2 IVH on the left. Heterogeneity suggests some aging of the clot. **b** US in the parasagittal plane shows prominent clot (*arrow*) as an echogenic area with some heterogeneity. Clot dilates the ventricle. It is seen anterior (*white arrowhead*) to the probable position of the foramen of Monro, confirming it is clot rather than choroid. It is also seen in the occipital horn (*black arrowhead*), another indicator of clot rather than normally echogenic choroid plexus

could also be caused by residual clot. When the clot dissolves, echogenic debris appears within the ventricular CSF, particularly in its dependent portions, e.g., the occipital horns in a supine neonate (Fig. 16). *Grade 4 hemorrhage* is an intraventricular hemorrhage with associated venous infarction. This hemorrhagic infarction appears as a brightly echogenic area in the periventricular white matter, which is usually ipsilateral to the associated IVH (Figs. 17 and 18). Periventricular hemorrhagic infarction can be unilateral or bilateral [20]. It can cavitate with formation of a porencephalic cyst (Fig. 19). In most cases with time the affected area fills in by gliosis and can no longer be distinguished as abnormal on US imaging.

Posterior fossa hemorrhage

Premature infants can develop cerebellar hemorrhage. Historically these have not been seen well at US

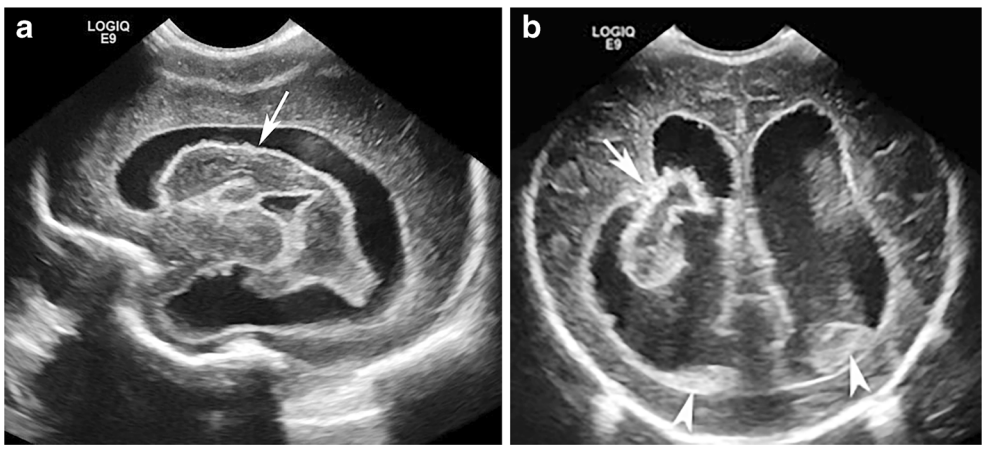

Fig. 15 Aging clot. Head US examination in a 4-week-old girl born at 24 weeks of gestation. **a** US in the right parasagittal plane shows clot (*arrow*) within a dilated lateral ventricle. Its position, both anterior to the expected foramen of Monro and posterior to the occipital horns, indicates that this is a clot and not choroid plexus. This is also evidenced by its peripheral bright echogenicity, with the remainder of the clot showing lesser echogenicity. The ventricular lining is hyperechoic, consistent with ventriculitis versus residual hemorrhage lining the ventricular walls. **b** US in the coronal plane shows irregularly shaped older clot (*arrow*), probably retracting in the moderately dilated right lateral ventricle. Note the clots (*arrowheads*) in the dependent portion of both lateral ventricles. These changes occurred over 4 weeks after the original diagnosis of IVH, when homogeneously echogenic hemorrhage was noted (not shown)

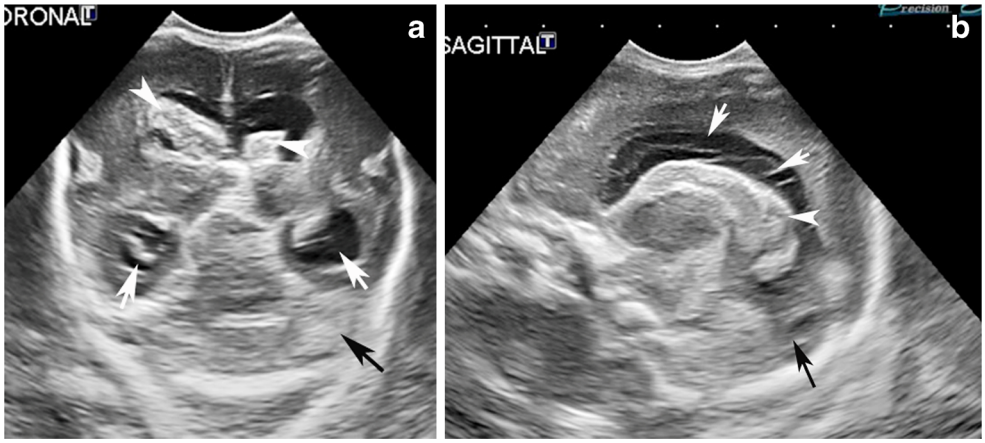

Fig. 16 Subacute older grade 3 intraventricular hemorrhage. Head US imaging in a 2-week-old boy born at 26 weeks of gestation. **a** US in coronal plane shows a large clot (*left arrowhead*) in a dilated right frontal horn. Note the smaller clot (*right arrowhead*) in the left frontal horn. The heterogeneity, including the brighter periphery of the clot, indicates that it is subacute or older. The temporal horn tips (*white arrows*) are dilated. There is question of a peripheral left cerebellar hemorrhage (*black arrow*). **b** US in the left sagittal plane shows clot as heterogeneous echogenicity, perhaps surrounding non-discernable choroid (*arrowhead*). Note the linear areas of echogenicity (*arrows*) in the upper portion of the ventricle, consistent with lace-like residua from the intraventricular hemorrhage and clot lysis, which are not usually seen. More typically seen is dependent intraventricular echogenicity (*black arrow*), consistent with debris from clot lysis

imaging with the anterior or even posterior fontanelle views. Mastoid views have helped. Cerebellar hemorrhage might be a result of prolonged labor and traumatic delivery. These hemorrhages are more common in preterm infants with extremely low birth weight (<750 g) [25]. It is believed that germinal matrix zones that exist within the subependymal layer of the 4th ventricle can bleed in preterm infants [26]. These infants present with unexplained motor agitation. They can have parenchymal or subarachnoid hemorrhage without IVH [27]. Acute cerebellar hemorrhage, as with any brain hemorrhage, appears homogeneously echogenic, but with time and clot lysis the appearance becomes heterogeneous, and eventually hypoechoic (Fig. 20). Hydrocephalus can develop in affected infants. Mastoid fontanelle views have led to improved detection of cerebellar hemorrhage because the vermis, cerebellar hemisphere and 4th ventricle are far nearer to a high-frequency transducer in the mastoid fontanelle and therefore are better seen compared to imaging via the standard anterior fontanelle window [12, 27].

Fig. 17 Grade 4 hemorrhage. Head US examination, coronal plane, in a 7-day-old girl born at 24 weeks of gestation. US shows a large echogenic mass (*arrow*) extending well beyond the expected superior extent of the right frontal horn. The left frontal horn can be used as a guide. The area involving the right frontal brain beyond the frontal horn is an associated white matter infarction that could eventually develop into an area of porencephaly. The right frontal hemorrhagic infarction creates an impression on the cavum septum pellucidum. There is clot in the left frontal horn

Post-hemorrhagic hydrocephalus

Post-hemorrhagic hydrocephalus is a clinically important sequela of IVH (Fig. 21). Neonates with acute post-hemorrhagic hydrocephalus might present with rapidly increasing head circumference, a tense anterior fontanelle, apnea, vomiting and abnormal posture. An obstruction inside the ventricular system proximal to the 4th ventricle outlets and the foramina of Luschka and Magendie is defined as noncommunicating hydrocephalus, whereas an obstruction outside the ventricular system is known as a communicating hydrocephalus. Most cases of post-hemorrhagic hydrocephalus are cases of communicating hydrocephalus, and this could be caused by chemical arachnoiditis developing from blood products and resulting in arachnoid granulation fibrosis and meningeal fibrosis, which impairs CSF absorption [28].

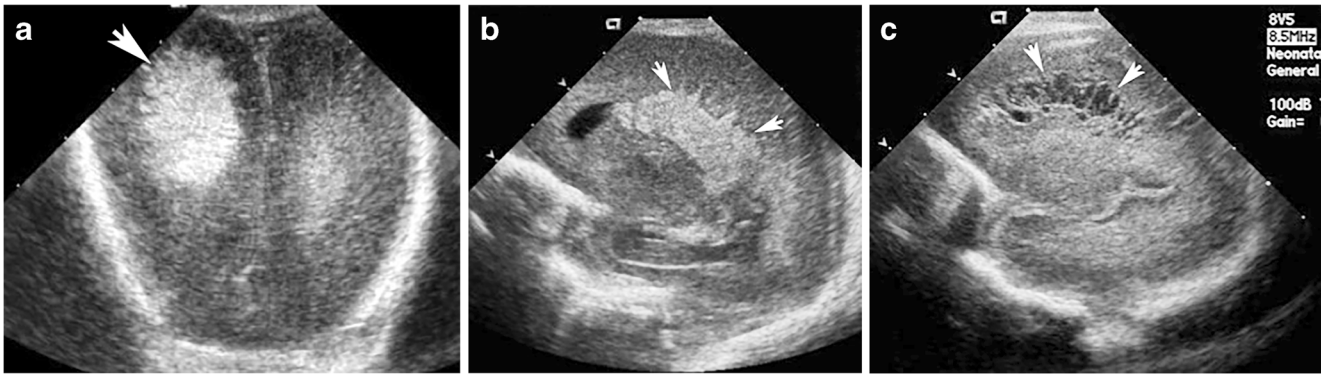

Fig. 18 Grade 4 hemorrhage evolving into cystic white matter infarction. Head US imaging in a 4-day-old boy born at 24 weeks of gestation. **a** US imaging in coronal plane shows a large bright echogenicity in the right parietal area, consistent with infarction. **b** Imaging in the right parasagittal plane shows clot as echogenicity in the dilated ventricle, but the linear areas of echogenicity (*arrows*) extending from it suggest white matter infarction beyond the ventricle. **c** US in the right parasagittal plane performed 2 weeks later shows cystic areas (*arrows*) in the right periventricular white matter, where previously there was bright echogenicity. This was the result of evolving infarction

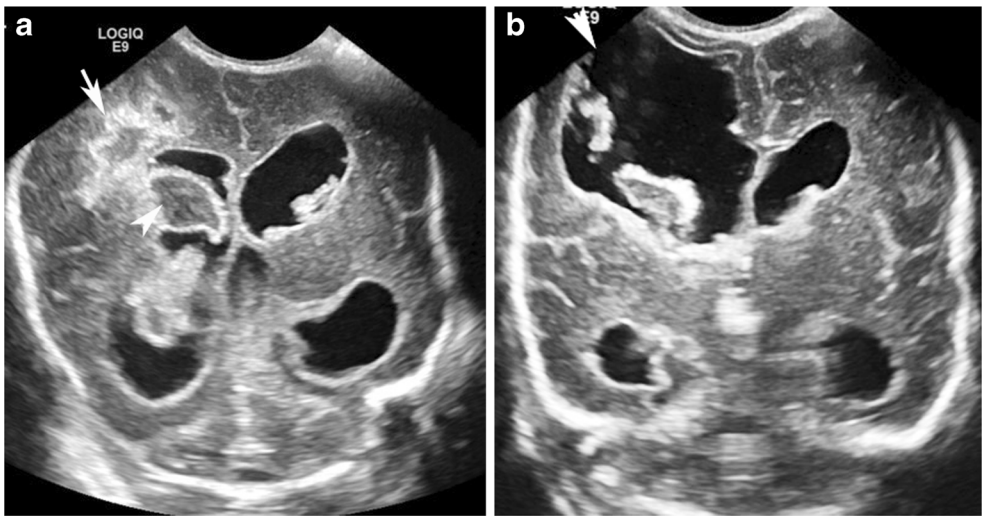

Fig. 19 Evolution of grade 4 hemorrhage into porencephalic cyst. Head US examination in the coronal plane in a 2-week-old girl born at 25 weeks of gestation. **a** US shows a heterogeneous area (*arrow*) in the right frontal parenchyma. There is older clot (*arrowhead*) in the right frontal horn. There is debris from hemorrhage in the left frontal horn. There is also moderate dilation of the lateral ventricles, including the temporal horns. **b** US performed several weeks later shows a large cystic area (*arrow*) extending from the frontal horn to the most superior aspect of the frontal brain. Aging clot and debris are seen within it. The abnormal brain seen in (**a**) cavitated over several weeks into a large porencephalic cyst, communicating with the right frontal horn

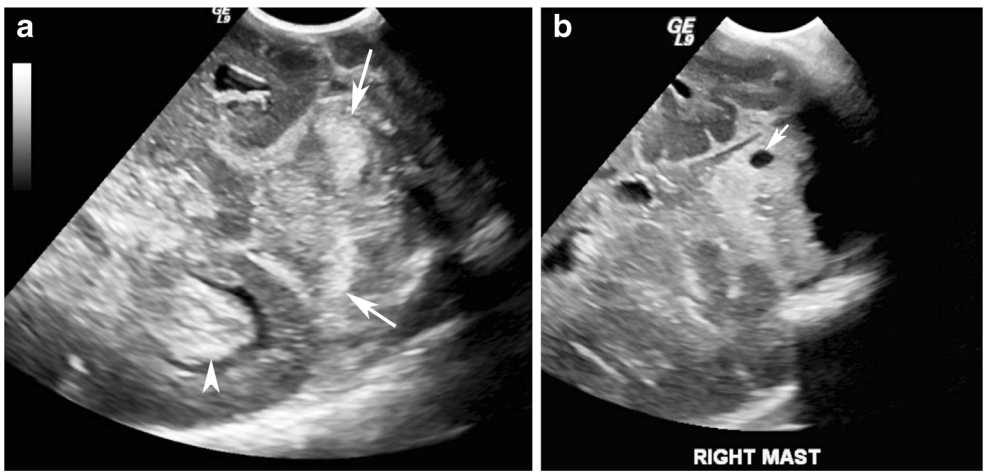

Fig. 20 Cerebellar hemorrhage and its evolution. Head US imaging, mastoid views, in a 4-day-old boy born at 26 weeks of gestation. **a** US shows right and left cerebellar hemisphere areas of echogenicity (*arrows*) consistent with intraparenchymal hemorrhage. Clot (*arrowhead*) within the dilated downside ventricle confirms that there was also supratentorial intraventricular hemorrhage. **b** US imaging performed 3 weeks later shows that part of the cerebellar hemorrhage became cystic (*arrow*)

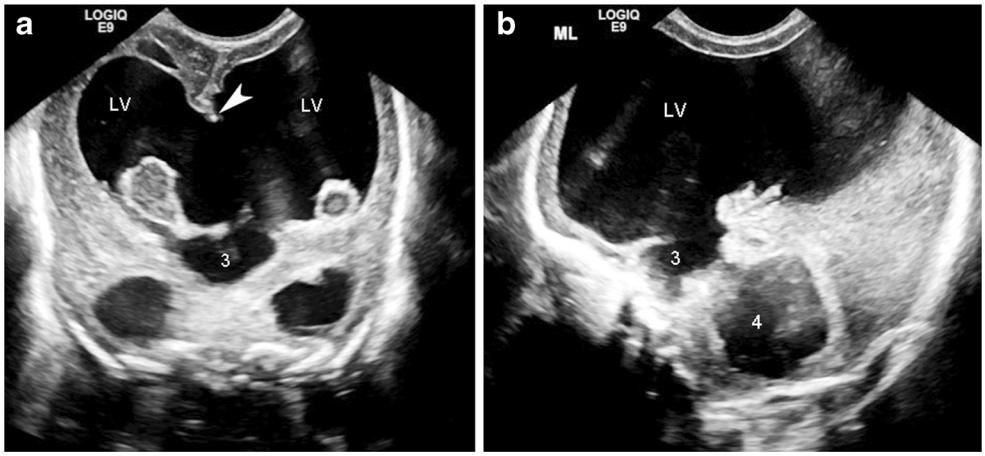

Fig. 21 Communicating post-hemorrhagic hydrocephalus. Head US examination in a 4-week-old boy born at 25 weeks of gestation. **a** Coronal plane US imaging shows that the lateral ventricles (*LV*) are much dilated and contain residual aging clot. The temporal horns are dilated. The dilated frontal horns extend via the foramina of Monro into a dilated 3rd ventricle (*3*). There is almost complete fenestration of the septi pellucidi because of the long-term hydrocephalus. Note the remnant of the septum pellucidum (*arrowhead*). **b** US imaging in sagittal plane. An oblique near-midline view shows the dilated lateral ventricle (*LV*), dilated 3rd ventricle (*3*) and very dilated 4th ventricle (*4*). The dilation of the ventricles could be caused by communicating hydrocephalus from an obstructing clot just beyond the foramina of Magendie and Luschka or from inflammation of the arachnoid villi, limiting the cerebrospinal fluid resorption

An inflammatory factor, transforming growth factor beta (TGF-B), has been implicated as a cause of post-hemorrhagic hydrocephalus by its stimulation and production of extracellular matrix, causing scarring and obstruction of arachnoid villi [29, 30]. Noncommunicating hydrocephalus can also occur secondary to obstruction of CSF flow within the ventricular system from blood clots or webs and synechiae that develop secondary to the hemorrhage. Sometimes obstruction can occur at both the aqueduct and the outlets of the 4th ventricle, resulting in a trapped 4th ventricle. This often requires an additional ventriculostomy because a ventriculoperitoneal shunt within the lateral ventricle only decompresses the lateral and 3rd ventricles and not the trapped 4th ventricle [31].

Most radiologists assess ventriculomegaly by gestalt rather than by a fixed set of measurements [12]. Some clinicians use bifrontal index measurements for shunt decisions. The bifrontal index is the width of the greatest span of the frontal horns divided by the greatest width of the inner diameter of the skull, and is usually less than 0.29 in normal neonates [32, 33]. Serial US imaging can help monitor ventricular dilation, to identify infants who require shunt placement [7]. Post-hemorrhagic hydrocephalus occurs in approximately 1% of infants with grade 1 IVH, 4% of those with grade 2, 25% of those with grade 3 and 28% of those with grade 4 [34]. Ventriculoperitoneal shunting, usually reserved for worsening ventriculomegaly over time, is performed in approximately 15% of neonates with post-hemorrhagic hydrocephalus [2]. US imaging is helpful in noting ventricular decompression in infants shunted for hydrocephalus. Historically, some researchers have used Doppler US and graded compression of the anterior fontanelle to evaluate neonatal hydrocephalus, suggesting the need for shunt placement when there was a 20% increase in resistive index or a reversal of diastolic flow in the spectral pattern obtained by insonating anterior cerebral and middle cerebral arteries [35, 36].

Hypoxic–ischemic injury in preterm neonates

Severe hypoxic events result in brain injury, most particularly in areas of advanced myelination, which have the highest metabolic activity [37, 38]. These areas include the thalami, globus pallidi, hippocampi, dorsal brainstem and the cerebellum. In premature infants, the caudate nucleus, putamen and the peri-Rolandic cortex are spared, as compared to term infants, because these areas myelinate only at a gestational ages of 35 weeks and older. US imaging has low sensitivity in detecting early ischemic changes in the deep structures of the brain. The most common US pattern is transient or persistent hyperechogenicity, which might progress to cavitation in the globus pallidus and ventral lateral nuclei of the thalamus [39, 40] (Fig. 22). These findings are best seen on MR. With more severe insults involving the cortex and subcortical white matter, US might depict indirect evidence of edema, such as effacement of the sulci, loss of gray–white matter differentiation, and compressed lateral ventricles. Cystic (cavitated) brain lesion can be picked up in the later phases on US. However, it is said that 50–70% of hypoxic–ischemic lesions seen on autopsy are missed at US [40]. MRI

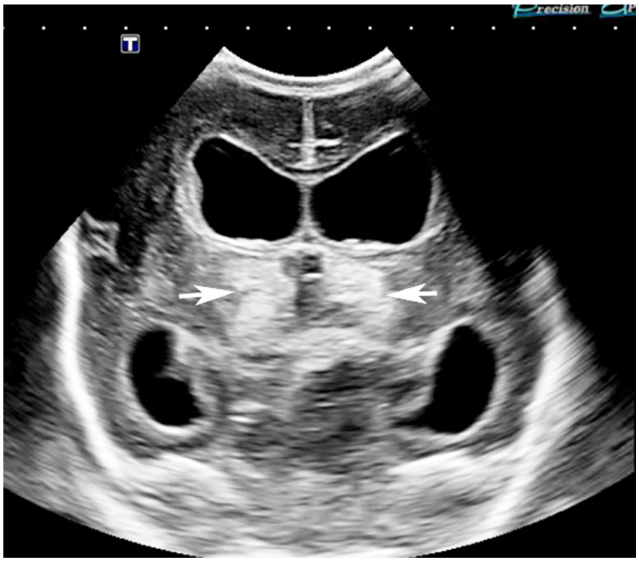

Fig. 22 Hypoxic–ischemic encephalopathy (HIE). Head US imaging in the coronal plane in a 10-day-old girl born at 23 weeks of gestation with HIE. US shows the prominent echogenicity in the bilateral thalami (*arrows*) with some heterogeneity, consistent with evolving changes of HIE. Post-hemorrhagic hydrocephalus with the dilation of the lateral ventricles and the 3rd ventricle is also seen secondary to evolving intraventricular hemorrhage. Echogenic clot and debris are seen in the frontal horns and the 3rd ventricle

of the brain allows better characterization of severe hypoxic–ischemic injury, particularly parenchymal abnormalities, which might be invisible on US because they do not have a cystic phase. Diffuse extensive high-signal-intensity lesions associated with HIE might only be seen on MRI, and in particular on diffusion-weighted sequences [40].

Periventricular leukomalacia

Periventricular leukomalacia (PVL) is a well-documented abnormality occurring in the brain of premature infants as a result of ischemic insult to the white matter tracts. In preterm infants of less than 32 weeks' gestational age, the periventricular white matter is in watershed areas, where the deep penetrating arteries have not yet developed. PVL is most commonly observed adjacent to the trigone of the lateral ventricles and in the white matter lateral to the frontal horns [12]. The cerebral white matter of the immature brain is populated predominantly by pre-oligodendrocytes, which are more susceptible to hypoxic injury as opposed to the mature oligodendrocytes of the term brain [38, 41, 42]. Long-term sequelae of PVL include visual, acoustic and motor deficits with spastic diplegia or quadriplegia [3, 11].

The first phase of PVL is manifested by increased echogenicity in the periventricular white matter from white matter edema or hemorrhage occurring predominantly lateral to the frontal horns or in the peritrigonal region [43] (Fig. 23). Hemorrhagic PVL has been shown to be much more common (64%) than once thought based on studies using MRI and US correlation [44, 45]. The echogenic phase of PVL can at times appear similar to the normal echogenic periventricular white matter. One should be suspicious for PVL when there is either unusually increased echogenicity or asymmetry to the periventricular echogenicity in the white matter. If unsure, a 2- to 3-week follow-up usually shows the development of periventricular white matter cysts in the area of concern if there was true echogenic PVL that evolved into cystic PVL. The cystic changes are usually bilateral and often symmetrical. The cysts can be single or multiple and tend to be seen parallel to the ventricular border in the deep white matter, again most commonly observed in watershed areas adjacent to the trigone of the lateral ventricles and lateral to the frontal horns [44] (Fig. 23). These cysts measure from millimeters to 1–2 cm in diameter. Thinning of the corpus callosum often follows PVL because of white matter necrosis or secondary axonal degeneration [44, 46]. These cysts can coalesce and merge with the adjacent ventricular wall, manifesting as irregular or wavy ventricular margins. With the passage of additional weeks to months the tiny cysts fill with fibrous and glial cells, and they sometimes completely disappear with gliosis and periventricular volume loss, the only indicator of abnormality [47, 48]. With the resultant white matter injury, generalized atrophy gradually sets in with widening of cerebral sulci, widening of the interhemispheric fissure and ex vacuo ventriculomegaly [49].

Timing and frequency of screening head US in preterm neonates

Based on what US imaging can detect, recommendations have been made to avoid missing cases of IVH and PVL in the asymptomatic newborn as well as the complications of post-hemorrhagic hydrocephalus in patients with known IVH. An initial scan is performed between days 3 and 7 after birth to capture IVH in the first week. A second scan between days 10 and 14 is thought to identify most clinically and developmentally important lesions [3, 12, 50]. The rationale behind this scan timing is the desire to identify IVH — which is noted in 75% cases in the first week of age and in at least 84% by days 10–14 — while at the same time noting whether there is development of any early

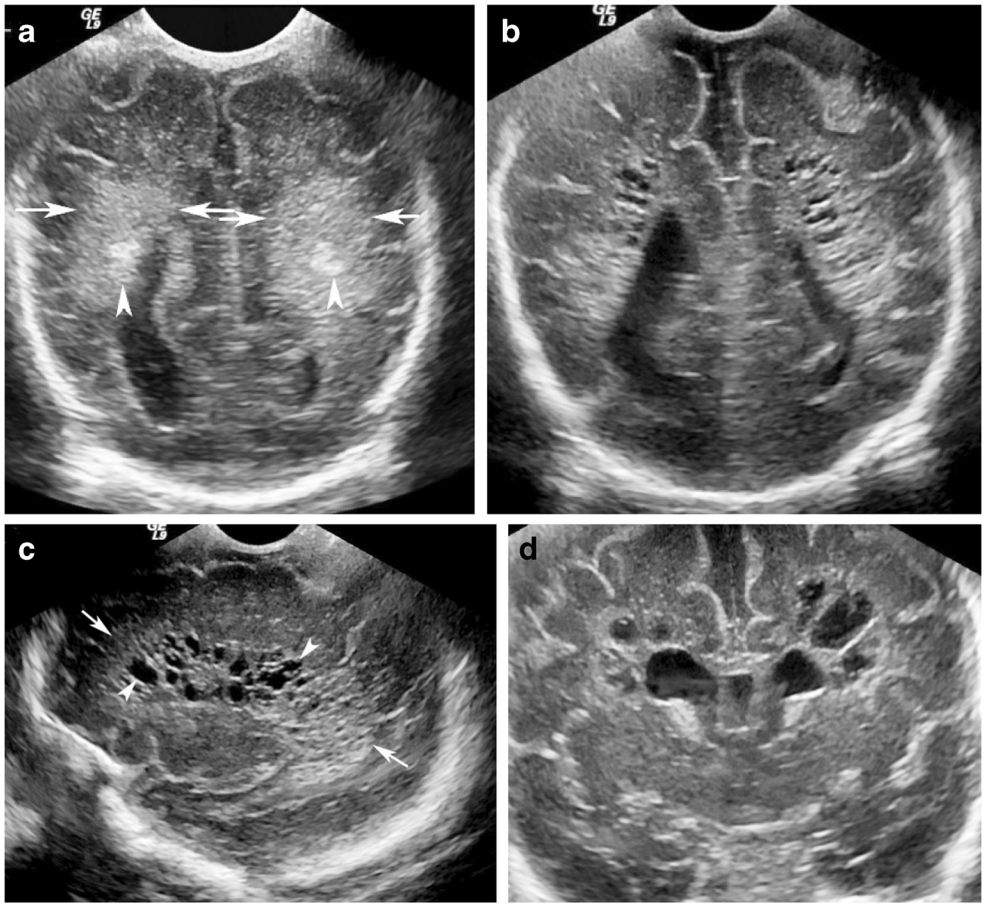

Fig. 23 Evolving periventricular leukomalacia (PVL). **a** Head US imaging in the coronal plane in a 14-day-old boy born at 31 weeks of gestation. US shows the relatively symmetrical but wider-than-normal periventricular white matter regions (*arrows*). Small contained areas of even brighter echogenicity (*arrowheads*) might be related to focal hemorrhage or edema. At this point echogenic PVL was considered. **b** Head US in the coronal plane 2 weeks later. Cystic areas are now seen in areas of previously noted homogeneously bright echogenicity, confirming the concern for PVL, now in its cystic phase and more readily diagnosable. **c** Left parasagittal plane US imaging shows cystic areas (*arrowheads*) within the echogenic white matter (*arrows*) in the peripheral left brain, consistent with cystic PVL. **d** US imaging in the coronal plane coned down to the frontal horn region shows cysts of PVL in the classic anterior watershed area, just lateral to the frontal horns. Again, these cysts that developed in echogenic periventricular areas confirm the suspicion of PVL

hydrocephalus or echogenic PVL [3]. A third scan might be performed at 4–6 weeks of age to exclude unexpected PVL and post-hemorrhagic hydrocephalus [3, 12]. Obviously in symptomatic neonates (e.g., dropping hematocrit, seizures) a head US examination should be performed as soon as possible. MRI is the imaging modality of choice for HIE in the acute phase because US has lower sensitivity for the detection of early ischemic changes [40, 45].

Conclusion

Head US imaging is an excellent screening tool and sometimes the only tool necessary for evaluating preterm neonates for intracranial hemorrhage and ischemic insults. With head sonography and follow-up US or correlative MR exams, it is possible to diagnose in a timely manner and allow for intervention when necessary. Intracranial US findings can help in predicting long-term neurodevelopmental outcomes.

Compliance with ethical standards

Conflicts of interest The authors have no financial interests, investigational or off-label uses to disclose.

References

1. O'Leary H, Gregas MC, Limperopoulos C et al (2009) Elevated cerebral pressure passivity is associated with prematurity-related intracranial hemorrhage. Pediatrics 124:302–309
2. Volpe JJ (2008) Intracranial hemorrhage: germinal matrix-intraventricular hemorrhage of the premature infant. In: Volpe JJ (ed) Neurology of the newborn, 5th edn. Saunders, Philadelphia, pp 517–588

3. Perlman JM, Rollins N (2000) Surveillance protocol for the detection of intracranial abnormalities in premature neonates. Arch Pediatr Adolesc Med 154:822–826
4. Burstein J, Papile L, Burstein R (1977) Subependymal germinal matrix and intraventricular hemorrhage in premature infants: diagnosis by CT. AJR Am J Roentgenol 128:971–976
5. Babcock DS, Han BK, LeQuesne GW (1980) B-mode gray scale ultrasound of the head in the newborn and young infant. AJR Am J Roentgenol 134:457–468
6. Ben-Ora A, Eddy L, Hatch G et al (1980) The anterior fontanelle as an acoustic window to the neonatal ventricular system. J Clin Ultrasound 8:65–67
7. London DA, Carroll BA, Enzmann DR (1980) Sonography of ventricular size and germinal matrix hemorrhage in premature infants. AJR Am J Roentgenol 135:559–564
8. Correa F, Enriquez G, Rossello J et al (2004) Posterior fontanelle sonography: an acoustic window into the neonatal brain. AJNR Am J Neuroradiol 25:1274–1282
9. Anderson N, Allan R, Darlow B et al (1994) Diagnosis of intraventricular hemorrhage in the newborn: value of sonography via the posterior fontanelle. AJR Am J Roentgenol 163:893–896
10. Cohen HL, Blitman NM, Sanchez (1996) Neurosonography of the infant: the normal examination. In: Ultrasonography of the prenatal and neonatal brain. McGraw-Hill, New York, pp 403–422
11. Shaw CM, Alvord EC Jr (1969) Cava septi pellucidi et vergae: their normal and pathogical states. Brain 92:213–223
12. Benson JE, Bishop MR, Cohen HL (2002) Intracranial neonatal neurosonography: an update. Ultrasound Q 18:89–114
13. Epelman M, Daneman A, Blaser SI et al (2006) Differential diagnosis of intracranial cystic lesions at head US: correlation with CT and MR imaging. Radiographics 26:173–196
14. Worthen NJ, Gilbertson V, Lau C (1986) Cortical sulcal development seen on sonography: relationship to gestational parameters. J Ultrasound Med 5:153–156
15. Enriquez G, Correa F, Lucaya J et al (2003) Potential pitfalls in cranial sonography. Pediatr Radiol 33:110–117
16. Buckley KM, Taylor GA, Estroff JA et al (1997) Use of the mastoid fontanelle for improved sonographic visualization of the neonatal midbrain and posterior fossa. AJR Am J Roentgenol 168:1021–1025
17. Volpe JJ (1989) Intraventricular hemorrhage in the premature infant — current concepts. Part I. Ann Neurol 25:3–11
18. Papile LA, Burstein J, Burstein R et al (1978) Incidence and evolution of subependymal and intraventricular hemorrhage: a study of infants with birth weights less than 1,500 gm. J Pediatr 92:529–534
19. Taylor GA (1995) Effect of germinal matrix hemorrhage on terminal vein position and patency. Pediatr Radiol 25:S37–S40
20. Bassan H, Feldman HA, Limperopoulos C et al (2006) Periventricular hemorrhagic infarction: risk factors and neonatal outcome. Pediatr Neurol 35:85–92
21. Vohr B, Allan WC, Scott DT et al (1999) Early-onset intraventricular hemorrhage in preterm neonates: incidence of neurodevelopmental handicap. Semin Perinatol 23:212–217
22. Cohen HL, Haller JO, Gross BR (1992) Diagnostic sonography of the fetus: a guide to the evaluation of the neonate. Pediatr Ann 21: 87, 91–86, 98–89
23. Elchalal U, Yagel S, Gomori JM et al (2005) Fetal intracranial hemorrhage (fetal stroke): does grade matter? Ultrasound Obstet Gynecol 26:233–243
24. Rypens E, Avni EF, Dussaussois L et al (1994) Hyperechoic thickened ependyma: sonographic demonstration and significance in neonates. Pediatr Radiol 24:550–553
25. Tam EWY, Rosenbluth G, Rogers EE et al (2011) Cerebellar hemorrhage on MRI in preterm newborns associated with abnormal neurological outcome. J Pediatr 158:245–250
26. Merrill JD, Piecuch RE, Fell SC et al (1998) A new pattern of cerebellar hemorrhages in preterm infants. Pediatrics 102:E62
27. Ecury-Goossen GM, Dudink J, Lequin M et al (2010) The clinical presentation of preterm cerebellar haemorrhage. Eur J Pediatr 169: 1249–1253
28. Robinson S (2012) Neonatal posthemorrhagic hydrocephalus from prematurity: pathophysiology and current treatment concepts. J Neurosurg Pediatr 9:242–258
29. Cherian S, Whitelaw A, Thoresen M et al (2004) The pathogenesis of neonatal post-hemorrhagic hydrocephalus. Brain Pathol 14:305–311
30. Lipina R, Reguli S, Novackova L et al (2010) Relation between TGF-beta 1 levels in cerebrospinal fluid and ETV outcome in premature newborns with posthemorrhagic hydrocephalus. Childs Nerv Syst 26:333–341
31. Hall TR, Choi A, Schellinger D et al (1992) Isolation of the fourth ventricle causing transtentorial herniation: neurosonographic findings in premature infants. AJR Am J Roentgenol 159:811–815
32. Levene MI (1981) Measurement of the growth of the lateral ventricles in preterm infants with real-time ultrasound. Arch Dis Child 56: 900–904
33. LeMay M (1984) Radiologic changes of the aging brain and skull. AJR Am J Roentgenol 143:383–389
34. Christian EA, Jin DL, Attenello F et al (2016) Trends in hospitalization of preterm infants with intraventricular hemorrhage and hydrocephalus in the United States, 2000-2010. J Neurosurg Pediatr 17:260–269
35. Taylor GA, Phillips MD, Ichord RN et al (1994) Intracranial compliance in infants: evaluation with Doppler US. Radiology 191: 787–791
36. Taylor GA (1992) Effect of scanning pressure on intracranial hemodynamics during transfontanellar duplex US. Radiology 185: 763–766
37. Grant PE, Yu D (2006) Acute injury to the immature brain with hypoxia with or without hypoperfusion. Magn Reson Imaging Clin N Am 14:271–285
38. Huang BY, Castillo M (2008) Hypoxic-ischemic brain injury: imaging findings from birth to adulthood. Radiographics 28:417–439
39. Sie LT, van der Knaap MS, Oosting J et al (2000) MR patterns of hypoxic-ischemic brain damage after prenatal, perinatal or postnatal asphyxia. Neuropediatrics 31:128–136
40. Furtado AD, Wisnowski JL, Painter MJ et al (2013) Neonatal brain injury. In: Coley BD (ed) Caffey's pediatric diagnostic imaging, 12 edn, vol 1. Elsevier, Philadephia, pp 284–298
41. Back SA, Luo NL, Borenstein NS et al (2001) Late oligodendrocyte progenitors coincide with the developmental window of vulnerability for human perinatal white matter injury. J Neurosci 21:1302–1312
42. Back SA (2015) Brain injury in the preterm infant: new horizons for pathogenesis and prevention. Pediatr Neurol 53:185–192
43. Grant EG, Schellinger D, Richardson JD et al (1983) Echogenic periventricular halo: normal sonographic finding or neonatal cerebral hemorrhage. AJR Am J Roentgenol 140:793–796
44. Rumack CM, Drose JA (2011) Neonatal and infant brain to imaging. In: Rumack CM, Wilson SR, Charboneau JW, Levine D (eds) Diagnostic ultrasound, 4th edn. Elsevier, Philadelphia, pp 1558–1636
45. Sie LT, van der Knaap MS, van Wezel-Meijler G et al (2000) Early MR features of hypoxic-ischemic brain injury in neonates with periventricular densities on sonograms. AJNR Am J Neuroradiol 21:852–861
46. Epelman M, Daneman A, Halliday W et al (2012) Abnormal corpus callosum in neonates after hypoxic-ischemic injury. Pediatr Radiol 42:321–330
47. Bowerman RA, Donn SM, DiPietro MA et al (1984) Periventricular leukomalacia in the pre-term newborn infant: sonographic and clinical features. Radiology 151:383–388

48. Flodmark O, Roland EH, Hill A et al (1987) Periventricular leukomalacia: radiologic diagnosis. Radiology 162:119–124
49. Grant EG, Schellinger D (1985) Sonography of neonatal periventricular leukomalacia: recent experience with a 7.5-MHz scanner. AJNR Am J Neuroradiol 6:781–785
50. Tudehope DI, Lamont AC (1998) Neonatal cranial ultrasound screening for intraventricular haemorrhage. J Paediatr Child Health 34:112–113